

Joint inversion of 2D resistivity and seismic travel time data to image saltwater intrusion over karstic areas

Hamdan A. Hamdan · Antonis Vafidis

Received: 29 March 2012 / Accepted: 27 July 2012 / Published online: 19 August 2012
© Springer-Verlag 2012

Abstract The simultaneous inversion of multiple geophysical data types has been proven to be a powerful tool to both improve subsurface imaging and help in the interpretation process. The main goal of this paper was to develop joint inversion strategies to provide improved resistivity and seismic velocity images for delineating saline water zones in karstic geological formations. The cross-gradient constraint approach was adopted to jointly invert resistivity and seismic first arrival data. The basic idea of this approach is to quantitatively estimate the structural similarity between resistivity and seismic velocity models, using the cross product of their gradients and to achieve a unified geological model which satisfies both data sets. Initially, synthetic data were employed to help develop a joint inversion strategy to be used over such complex geological structures. The proposed strategy uses a weighting factor for the cross-gradient constraints and separate damping factors for the resistivity and seismic data. This strategy was applied successfully on field data from the karstic region of Stilos, Crete, Greece.

Keywords Joint inversion · Cross-gradient · Seawater intrusion · Electrical tomography · Seismic tomography

Introduction

Tomography, a well-known technique, is widely used to delineate the spatial distribution of the physical properties

of the geological formations such as resistivity and seismic velocity. In particular, electrical tomography, due to its sensitivity to the presence of ions, images effectively saline water zones in coastal areas (Gnanasundar and Elango 1999; Abdul Nassir et al. 2000; Imhof et al. 2001; Lashkaripour 2003; Singh et al. 2004; Kuras et al. 2005; Ogilvy et al. 2009).

On the other hand, imaging the geological formations, especially faults and fractured zones, is of great importance in understanding the saline water intrusion mechanism. Such information can be obtained using seismic methods (Haeni 1986; Mela 1997; Jarvis and Knight 2002). The combination of electrical and seismic tomography is probably the most appropriate methodology to image fresh and saline water zones in coastal areas (Sumanovac and Weisser 2001; Balia et al. 2003).

However, it is often hard to find a geological scenario which satisfies both resistivity and seismic velocity models. Simultaneous inversion techniques have been proposed to produce a unified model and reduce the ambiguities in geophysical interpretation (Vozof and Jupp 1975; Lines et al. 1988; Dobroka et al. 1991). The joint inversion of different data sets has already been applied in cases where these depend on the same physical parameter, such as data from dc resistivity and transient electromagnetic methods (Raiche et al. 1985; Sandberg 1993; Maier et al. 1995; Schmutz et al. 2000; Albouy et al. 2001; Athanasiou et al. 2007).

When the datasets depend on different physical parameters, joint inversion either utilizes experimental relationships between the petrophysical properties (Berge et al. 2000; Tillman and Stocker 2000) or the structural similarity of the geophysical models. An essential condition in the latter case is that the geophysical methods detect the same layers (Hering et al. 1995; Lines et al. 1988).

H. A. Hamdan (✉) · A. Vafidis
Laboratory of Applied Geophysics, Department of Mineral
Resources Engineering, Technical University of Crete,
73 100 Chania, Crete, Greece
e-mail: hamdangeoph@gmail.com

The joint inversion of electric and seismic tomography data maintains the common structural boundaries between the two models (structural approach) by employing a gradient operator (Zhang and Morgan 1997; Haber and Oldenburg 1997; Gallardo and Meju 2003, 2004). In this paper, a joint inversion algorithm for electric and seismic tomography is developed and tested on both synthetic and real data. The efficiency of this algorithm in imaging saline water zones in complex karstic geological formations is also examined.

Formulation of the joint inversion algorithm

Geophysical data inversion aims at finding model parameters which will reproduce the measured data. In this inversion procedure, it is necessary to solve the forward problem. Several techniques have been proposed to study the resistivity and seismic forward problems, which are usually based on numerical methods.

In this paper, a 2.5D finite element method (Tsourlos 1995; Tsourlos et al. 1998) approach was adopted to solve the resistivity forward problem. This approach gives better estimates of the apparent resistivity, compared to the conventional 2D method, since a 3D potential field is considered (Dey and Morrison 1979).

An optimized ray bending method solves the seismic forward problem using beta-splines for the ray parameterization. The 2.5D approach employs a small size third dimension axis (Moser 1991; Soupios et al. 2001).

Resistivity and seismic forward modeling involves nonlinear equations. By applying a first-order Taylor expansion, one can get a set of two linear equations:

$$f_r(m_r) \cong f_r(m_{0r}) + J_r(m_r - m_{0r}) \quad (1)$$

$$f_s(m_s) \cong f_s(m_{0s}) + J_s(m_s - m_{0s}) \quad (2)$$

where m_{0r} and m_{0s} are the initial resistivity and seismic velocity models, respectively, while J_r , J_s are Jacobian matrices. For the resistivity method, the Jacobian matrix J_r is estimated using the adjoint equation technique (Tsourlos 1995; McGillivray and Oldenburg 1990; Park and Van 1991), where the sensitivities are calculated as a function of an adjoint field (the adjoint Green's function) and the electric field for every model cell. The Jacobian matrix J_s is calculated by finding the ray length in each cell.

The next step uses an optimization method which minimizes the differences between the theoretical and the measured data. In geophysics, this is achieved by using the least squares method. A smoothness constraint (Constable et al. 1987) is added to the objective equation in order to regularize the ill-posed inversion problem:

$$\min \left\{ \Phi(m_r) = \|d_r - f_r(m_r)\|_{C_{ddr}^{-1}}^2 + \|\alpha_r Dm_r\|^2 \right\} \quad (3)$$

$$\min \left\{ \Phi(m_s) = \|d_s - f_s(m_s)\|_{C_{dds}^{-1}}^2 + \|\alpha_s Dm_s\|^2 \right\} \quad (4)$$

where d is the measured data (d_r : the logarithm of the apparent resistivities, d_s : the seismic travel times), f is the response of the model, ($f_r(m_r)$: the computed apparent resistivities, $f_s(m_s)$: the computed travel times), D is the smoothness matrix, α_r and α_s are the weighting coefficients which define the smoothing level of the models m_r and m_s , respectively, and C_{ddr} and C_{dds} are the covariance matrices of the electric and seismic data, respectively.

To simultaneously invert resistivity and seismic data, a common mesh for both models is necessary. Here, this mesh was created for the finite element resistivity forward problem and is subsequently used by the ray tracing algorithm. The resulting resistivity and seismic velocity models are considered structurally identical when their gradient vectors have the same or opposite direction. This can be expressed mathematically by the product of their gradients (Gallardo and Meju 2003, 2004):

$$\vec{t}(x, z) = \nabla m_r(x, z) \times \nabla m_s(x, z) = 0 \quad (5)$$

where \vec{t} is the cross-gradient vector, and m_r and m_s are the resistivity and seismic velocity models, respectively. This equation is of great importance in guiding the joint inversion procedure. Thus, the least squares joint inversion becomes:

$$\min \left\{ \Phi(m_r, m_s) = \left\| \begin{matrix} d_r - f_r(m_r) \\ d_s - f_s(m_s) \end{matrix} \right\|_{C_{dd}^{-1}}^2 + \left\| \begin{matrix} \alpha_r Dm_r \\ \alpha_s Dm_s \end{matrix} \right\|^2 \right\}, \quad (6)$$

$$\text{subject to } \vec{t}(m_r, m_s) = 0.$$

To satisfy the cross-gradient constraint ($\vec{t}(m_r, m_s) = 0$), the gradient vectors must be parallel (same or opposite direction) at points where variation in the physical parameters (resistivity and velocity) occurs. This means that the boundaries of the geological layers, detected by both methods, are located at the same position. The cross-gradient constraint $\vec{t}(m_r, m_s)$ (m_r, m_s) is linearized using the first-order Taylor expansion:

$$\vec{t}(m_r, m_s) \cong \vec{t}(m_{0r}, m_{0s}) + J_c \begin{pmatrix} m_r - m_{0r} \\ m_s - m_{0s} \end{pmatrix} \quad (7)$$

where J_c is the cross-gradient Jacobian matrix, which expresses derivatives of t with respect to the resistivity and seismic velocity. The values of J_c are calculated using finite differences (Gallardo and Meju 2004).

The objective Eq. (6) is solved by using Lagrange multipliers (Menke 1989). Here, we introduce a weighting

factor w_n (n denotes iteration number) in the formulation proposed by Gallardo and Meju (2004):

$$m = N_1^{-1}n_2 - w_n N_1^{-1} J_c^T \Lambda \tag{8}$$

$$\Lambda = (J_c N_1^{-1} J_c^T)^{-1} (J_c N_1^{-1} n_2 - J_c m_0 + t_0) \tag{9}$$

where N_1 and n_2 are calculated using the equations:

$$N_1 = \begin{bmatrix} \frac{1}{\beta_r^2} J_r^T C_{rr}^{-1} J_r + \alpha_r^2 D^T D & 0 \\ 0 & \frac{1}{\beta_s^2} J_s^T C_{ss}^{-1} J_s + \alpha_s^2 D^T D \end{bmatrix} \tag{10}$$

$$\text{and } n_2 = \begin{bmatrix} \frac{1}{\beta_r} J_r^T C_{rr}^{-1} \{d_r - f_r(m_{0r}) + J_r m_{0r}\} \\ \frac{1}{\beta_s} J_s^T C_{ss}^{-1} \{d_s - f_s(m_{0s}) + J_s m_{0s}\} \end{bmatrix} \tag{11}$$

and β_r, β_s are auxiliary damping factors for the resistivity and seismic components in (10) and (11), while Λ is the cross-gradient Lagrange multiplier used to determine the contribution percentage of the cross-gradient constraint in the inversion procedure. The first part of Eq. (8) describes the independent inversion of resistivity and seismic models, while the second part represents the cross-gradient constraint which is controlled by the Lagrange multiplier Λ .

In this approach, the original equations proposed by Gallardo and Meju (2004) are modified as follows:

- A weighting factor w_n introduced in Eq. (8) takes values between 0 and 1. When $w_n = 0$, the resistivity and seismic data are inverted independently. For $w_n = 1$, joint inversion is chosen. The inversion process usually begins with $w_n = 0$ at the first iteration. Afterward, the cross-gradient constraint is gradually introduced in the inversion process by increasing the value of w_n .
- The auxiliary damping factor β in the original equations is replaced by two factors corresponding to the resistivity β_r and the seismic β_s components. If $\beta_s > \beta_r$, the cross-gradient constraint is more sensitive to the resistivity data set, and thus the final outcome from the joint inversion is biased toward the resistivity model. These factors are very useful in cases where one of the two methods gives better images (e.g., karstic structures).
- An A priori model is not used in the objective Eq. (6). This is usually the case in the absence of boreholes.

Model with limestone block

This model consists of a marly limestone block surrounded by clays. The dimensions of this 2D model (Fig. 1a) are 40×10 m. The resistivity and P-wave velocity of the

clays are $10 \Omega \text{ m}$ and $1,000 \text{ m/s}$, respectively. The 6×3 -m marly limestone block buried at a depth of 2 m exhibits a resistivity of $100 \Omega \text{ m}$ and a velocity of $2,000 \text{ m/s}$.

Synthetic apparent resistivity data are generated by the finite elements (FE) algorithm (Tsourlos et al. 1998) using the dipole–dipole array (41 electrodes). The dipole distance a was set to 1 m, while the distance between the two dipoles was set to na where $n = 1, 2, \dots, 21$. The ray tracing method (Soupios et al. 2001) generated first arrivals for 39 geophone (receiver spacing = 1 m) and seven seismic shot points (source spacing = 5 m) (Fig. 1a).

The resistivity and seismic inversion are initially applied (Fig. 1b). The resistivity model was properly reconstructed after nine iterations. The resistivity values in the karstified marly limestone block, as well as the resistivity values of the surrounding clays, are very close to the actual ones. The inversion of the seismic data on the other hand, as expected, was not equally acceptable. The first arrivals correspond to seismic rays refracted from the top of the marly limestone block. Thus, the ray coverage within the limestone block is inadequate, resulting in imaging only the shallow part of the block which is misplaced (shifted upward).

Using the same value for both damping factors (β_r, β_s), the joint inversion algorithm exhibits increased root mean square (RMS) errors (Fig. 1c). In particular, the resistivity values in the marly limestone block are overestimated ($300\text{--}500 \Omega \text{ m}$). On the other hand, a high velocity zone is present close to the surface and the velocity in the block is underestimated at $1,300\text{--}1,600 \text{ m/s}$.

The fact that the limestone block is better imaged by the independent resistivity inversion indicates that more weight should be assigned to the resistivity data in the joint inversion. Increasing the value of the damping factor β_s in Eqs. (10) and (11) improved significantly the joint inversion (Fig. 1d). The damping factor β_s was assigned a value 28 in the first iteration, which decreased gradually to 1 over the first seven iterations, while factor β_r was kept as 1. The marly limestone block is better imaged here. However, the block’s resistivity is again overestimated.

To further improve these images, one can start with independent inversion, followed by the gradual introduction of the cross-gradient constraint. This strategy uses $w_n = 0$ in the first iteration, then increases subsequently to unity. This resulted in resistivity and velocity images (Fig. 1e) exhibiting structural similarity. The seismic velocities from this strategy show reduced RMS errors.

For the proposed joint inversion strategy, convergence is faster compared to the equally weighted cross-gradient inversion. This test shows that the joint inversion better reconstructs the resistivity and seismic velocity images. The use of the weighting factor w_n and the auxiliary damping factors (β_r, β_s) improved significantly the performance of the cross-gradient method (Fig. 2).

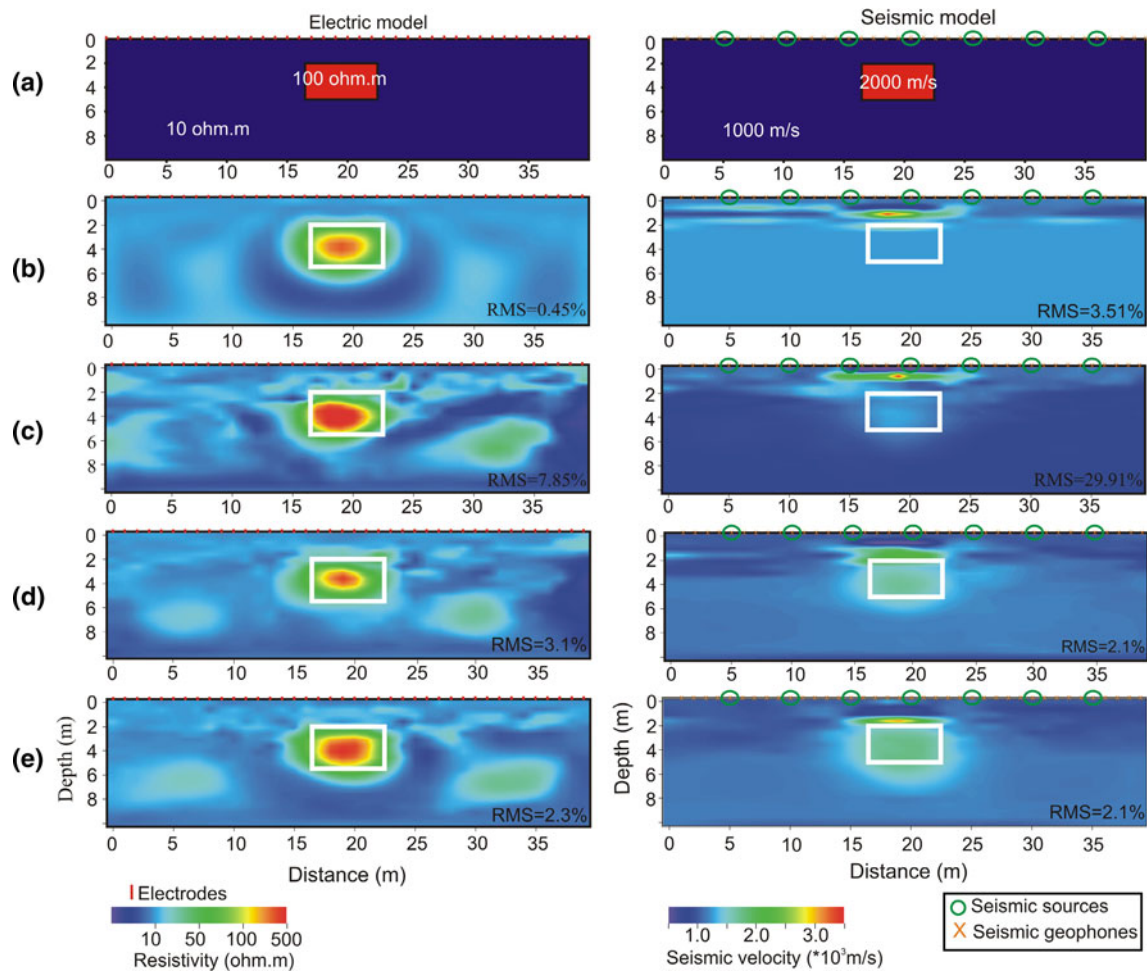


Fig. 1 Model 1: **a** the resistivity model is on the *left* and the seismic velocity model is on the *right*. **b** Independent smoothness constraint inversion sections. **c** Joint inversion sections: $\beta_r = \beta_s$. **d** Joint

inversion sections: $\beta_r < \beta_s$. **e** Joint inversion sections: $\beta_r < \beta_s$, where w_n gradually increases by 20 % per iteration. The *white frame* indicates the location of the marly limestone block

Model with saline water zone

This 2D model (40×10 m) consists of two layers (Fig. 3a). The thickness of the shallow layer is 3 m and its resistivity is 40Ω m, while its velocity is 1,200 m/s. These are typical values for marls observed in the region of Stylos, Chania. The deeper layer exhibits higher resistivity (150Ω m) and velocity (2,000 m/s) values typical for saturated marly limestones. A saline water zone is also present in the marly limestones. In this zone, the resistivity is very low (10Ω m), while the seismic velocity remains the same. This is an appropriate model for testing the cross-gradient joint inversion, since the velocity model encounters less interfaces compared to the electric one.

Synthetic apparent resistivity data and first arrival seismic data were calculated using the same survey parameters as in model 1 (Fig. 1). Random noise with normal distribution and standard deviation of 5 % was added. Figure 3b

shows the outcome of the independent inversion (four iterations). This geoelectric section indicates that the resistivity values approach the actual ones, but the thickness of the shallow layer is underestimated (2 m instead of 3 m). Seismic velocities are also in agreement with the actual ones.

Applying the cross-gradient joint inversion, the resistivity of the geoelectric layers and the thickness of the shallow layer on the geoelectric section are correctly estimated (Fig. 3c, four iterations). The resistivity images of the independent and joint inversion are similar. This is reasonable since high values were assigned to the damping factor β_s (60 in the first iteration and decreasing gradually to 1 over the first nine iterations while factor β_r was kept as 1). In the velocity image resulting from the cross-gradient joint inversion, the thickness of the shallow layer is more accurately estimated and the structural similarity between the resistivity and velocity sections is improved.

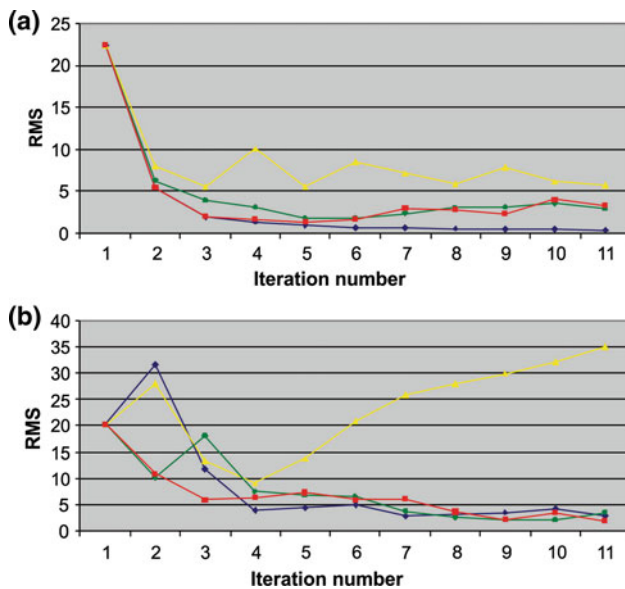


Fig. 2 RMS errors for the resistivity (a) and seismic (b) data for Model 1. Blue corresponds to the independent inversion, yellow to the joint inversion ($\beta_r = \beta_s$), green to the cross-gradient constraint joint inversion ($\beta_r < \beta_s$) and red to joint inversion ($\beta_r < \beta_s$, w_n gradually increases by 20 % per iteration)

Application to real data

The proposed joint inversion strategy was applied in the region of Stilos, Crete, Greece (Fig. 4). Exploration boreholes and natural springs revealed saline water, at a distance of 1–3 km from the seashore. This region is strongly

karstified and consists mainly of alluvium, marls and marly limestones.

Extensive geological and geophysical studies were conducted in the region of interest (Michalakis et al. 2006; Hamdan and Vafidis 2009; Hamdan et al. 2010; Soupios et al. 2010) and involved 11 electrical tomography lines (3.5 km) and 17 seismic tomography lines (3.5 km). The aim of this survey was to study the main mechanisms responsible for saline water intrusion and more specifically to examine the contribution of a major NE–SW fault in the saline water intrusion. The developed algorithm was applied on data from two survey lines.

Line 1

This line is located in the southwest part of the survey region, where karstified marly limestones outcrop. The Wenner–Schlumberger array, using 28 electrodes and electrode spacing of 7 m (189 m total length), was deployed. The resistivity section from the independent inversion (Fig. 5) indicates three geoelectric layers. These layers are attributed to unsaturated karstified marly limestones, saturated with freshwater and saturated but less karstified.

The corresponding seismic tomography employed five shot points (sledgehammer) in three 12-geophone spreads and 5-m geophone spacing. The seismic velocity section from independent inversion also suggests the existence of three seismic layers (Fig. 5). Here, the first and second

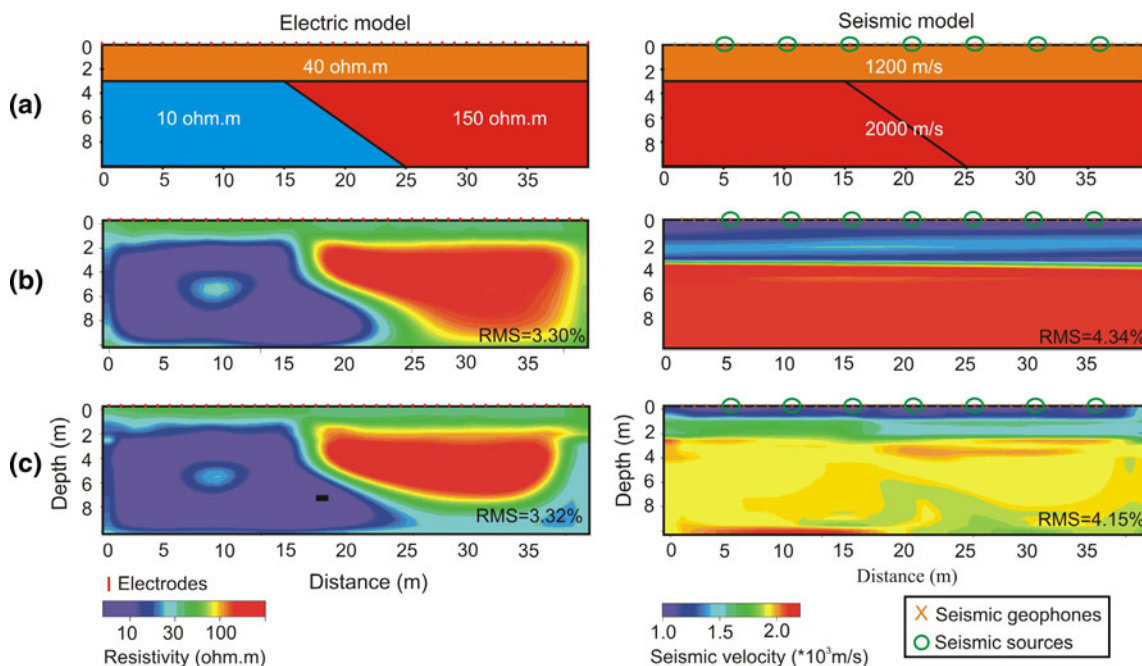


Fig. 3 Model 2: a the resistivity model is on the left (41 electrodes at every 1 m) and the seismic model is on the right. b Independent smoothness constraint inversion; c joint inversion ($\beta_r < \beta_s$) where w_n gradually increases by 20 % per iteration

Fig. 4 Geological map of the surveyed area showing the location of the resistivity (red color) and seismic (purple color) tomography lines

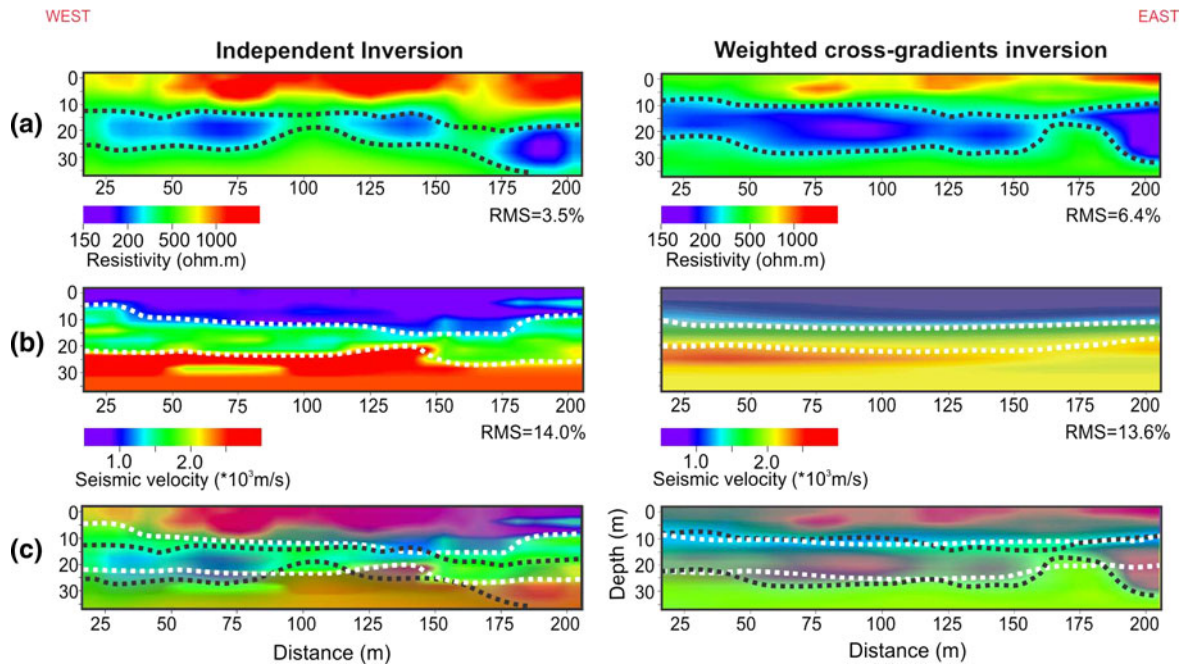
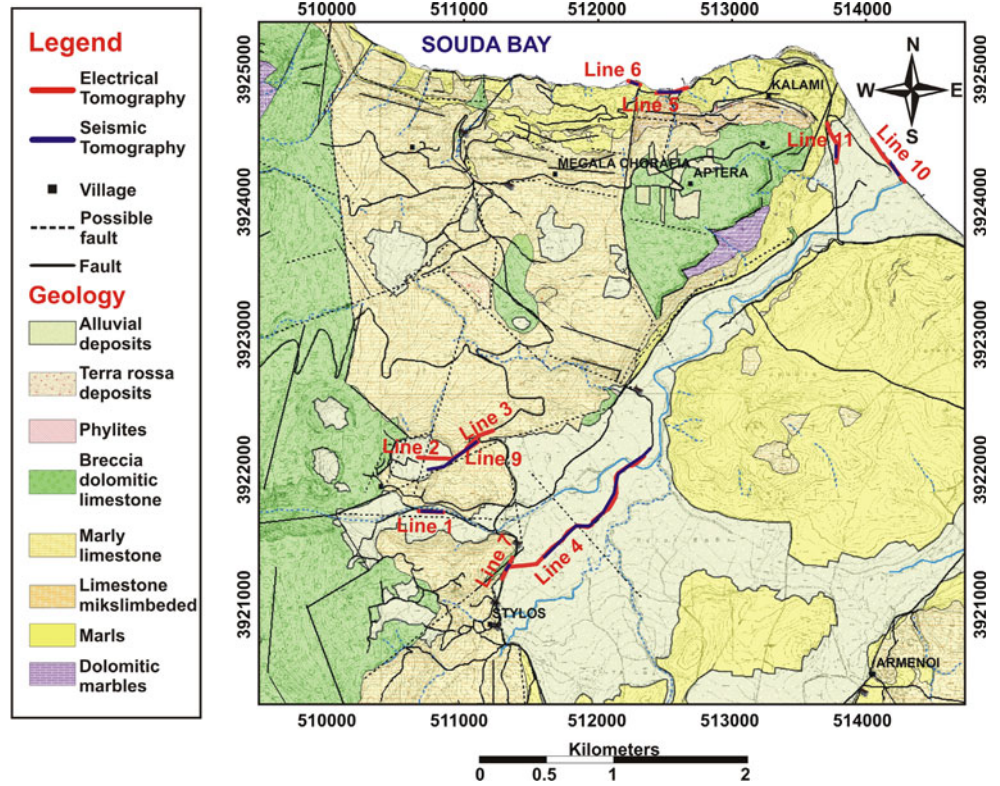


Fig. 5 Comparison of the independent inversion sections (left) and cross-gradient joint inversion sections (right) for line 1. **a** The resistivity sections, **b** the seismic sections and **c** the result of

superimposing the resistivity section over the seismic one. The dashed black line indicates the boundaries of the geoelectric zones, while the white one indicates the seismic velocity boundaries

layers are assigned to karstified and less karstified marly limestone. The third layer is attributed to Tripoli carbonates.

The independent inversion sections showed differences in the thickness of resistivity and seismic layers. In particular, there is a pronounced discrepancy at horizontal

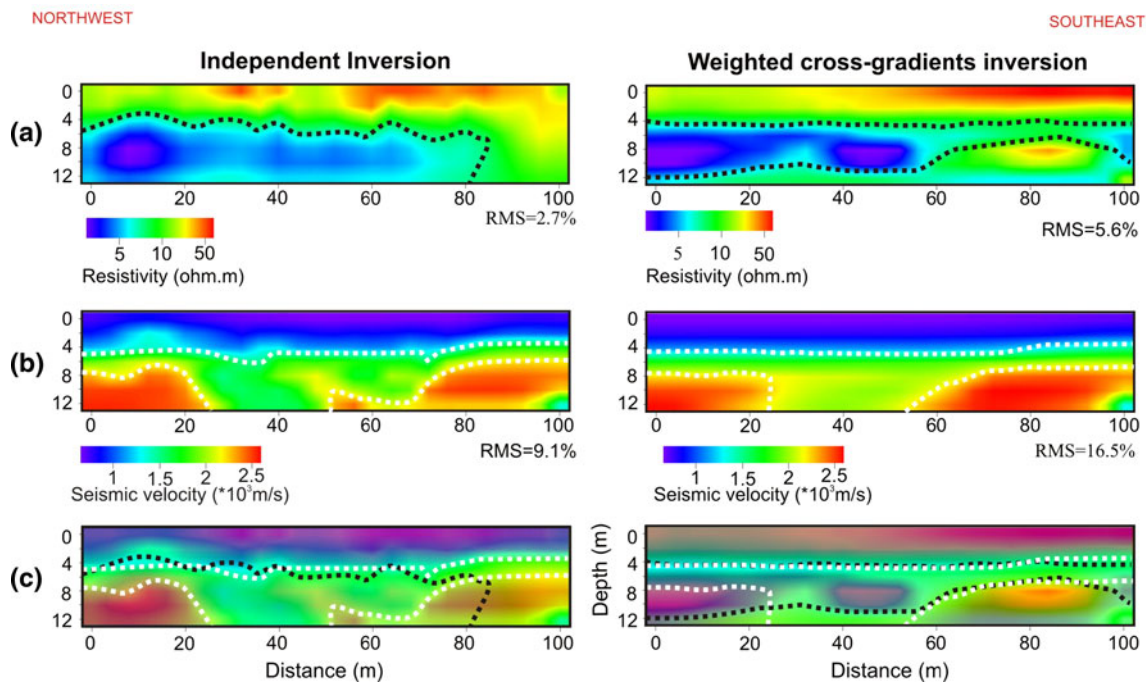


Fig. 6 Comparison of the independent inversion sections (*left*) and cross-gradient joint inversion sections (*right*) for line 6. **a** The resistivity sections, **b** the seismic sections and **c** the result of

superimposing the resistivity section over the seismic one. The *dashed black line* indicates the boundaries of the geoelectric zones, while the *white one* indicates the seismic velocity boundaries

distances greater than 175 m, where there is a lack of resistivity data, which is partially reduced by the joint inversion. The cross-gradient joint inversion algorithm and the proposed strategy improved the structural similarity between the two sections (Fig. 5c) indicating that the depth of the water table is approximately 10 m and the geological formations present at depths less than 35 m are karstified marly limestones and not Tripoli carbonates.

between these sections is the third seismic zone which is observed at the edges of the seismic section.

The resistivity section from the cross-gradient inversion shows a third higher resistivity layer. Better structural similarity between the two sections has been achieved, indicating the presence of seawater intrusion in the second and third layers.

Line 6

Discussion and conclusions

Line 6 is close to the seashore (at an elevation of 4 m). The resistivity data were collected using the Wenner–Schlumberger array deploying 27 electrodes with 4-m spacing (104 m in total length). One spread with five seismic shot points and 12 geophones was used for the corresponding seismic tomography. Marls are observed on the surface, while marly limestones are expected at shallow depths. A relatively high concentration of salts (>1,000 ppm) was detected in a spring about 300 m to the east of this line.

Two new strategies for joint inversion of resistivity and seismic data using cross-gradient are proposed and evaluated using synthetic datasets over the complex structures. In the case of model 1, the joint inversion significantly improved the seismic velocity section. One can dispute the advantages of using the joint inversion, since the independent resistivity inversion gives better results and exhibits lower RMS values. Nevertheless, achieving a unified model, for both seismic and electric data, might be of greater importance in the interpretation process, especially in geological conditions where it is difficult to decide which method is more reliable. The proposed strategies helped improving the joint inversion images by using a weighting factor and different values for the seismic and electric damping factors.

In the resistivity section (from the independent inversion after five iterations), low and very low resistivity zones are attributed to marls (top) and saturated marly limestone (probably seawater intrusion, Fig. 6), respectively. The seismic section, on the other hand, revealed three seismic layers attributed to marls (low velocities) and marly limestones. The first layer has the same thickness in both the resistivity and seismic sections. The main difference

The case of model 2 is more difficult since the seismic and resistivity models do not share the same (structural)

layers. Nevertheless, by increasing the difference between the seismic and electric auxiliary damping factors (β_r , β_s), the cross-gradient scheme successfully improved the structural similarity between both sections.

The application of the cross-gradient joint inversion proved to be very useful in the interpretation of the field data from the Stilos region. The independent inversion sections showed differences in the thickness of the geological layers, while the joint inversion section gave a more reasonable geological scenario. Specifically, in line 1, the joint inversion produced a better image of the subsurface and clarified the absence of Tripoli carbonates at the survey depths. In line 6, the joint inversion showed an additional less karstified marly limestone layer. These results emphasize the importance of the joint inversion in the interpretation process. Thus, joint inversion facilitates and speeds up the interpretation and in some cases the number of required verification boreholes is reduced.

Acknowledgments The authors are grateful to Dr. Panayiotis Tsourlos and Dr. Pantelis Soupios for providing their codes. They also wish to thank Mr. Nikos Andronikidis, Dr. Nikos Economou and Dr. George Kritikakis, collaborators at TUC, for the great help during the field data acquisition. This paper is part of the 03ED375 Research Project, implemented within the framework of the “Reinforcement Programme of Human Research Manpower” (PENED) and co-financed by National and Community Funds (25 % from the Greek Ministry of Development General Secretariat of Research and Technology and 75 % from E.U. European Social Fund).

References

- Abdul Nassir SS, Loke MH, Nawawi MN (2000) Salt-water intrusion mapping by geoelectrical imaging surveys. *Geophys Prospect* 48:647–661
- Albouy Y, Andrieux P, Rakotonondrasoa G, Ritz M, Descloitres M, Join JL, Rasolomanana E (2001) Mapping coastal aquifers by joint inversion of DC and TEM soundings—three case histories. *Groundwater* 39:87–97
- Athanasioiu EA, Tsourlos PI, Papazachos CB, Tsokas GN (2007) Combined weighted inversion of electrical resistivity data arising from different array types. *J Appl Geophys* 62:124–140
- Balia R, Gavaudo E, Ardaù F, Ghiglieri G (2003) Geophysical approach to the environmental study of a coastal plain. *Geophysics* 68:1446–1459
- Berge PA, Berryman JG, Bertete-Aguirre H, Bonner P, Roberts J, Wildenschild D (2000) Joint inversion of geophysical data for site characterization and restoration monitoring. LLNL rep. URCL-ID-128343. Proj. 55411, Lawrence Livermore Natl. Lab., Livermore
- Constable SC, Parker RL, Constable CG (1987) Occam’s inversion: a practical algorithm for generating smooth models from electromagnetic sounding data. *Geophysics* 52:289–300
- Dey A, Morrison HF (1979) Resistivity modeling for arbitrary shaped three-dimensional shaped structures. *Geophysics* 44:753–780
- Dobroka M, Gyulai A, Ormos T, Csokas J, Dresen L (1991) Joint inversion of seismic and geoelectric data recorded in an underground coal mine. *Geophys Prospect* 39:643–665
- Gallardo LA, Meju MA (2003) Characterization of heterogeneous near-surface materials by joint 2D inversion of DC resistivity and seismic data. *Geophys Res Lett* 30:1658. doi:10.1029/2003GL017370
- Gallardo LA, Meju MA (2004) Joint two-dimensional DC resistivity and seismic travel time inversion with cross-gradients constrains. *J Geophys Res* 109:B03311. doi:10.1029/2003JB002716
- Gnanasundar D, Elango L (1999) Groundwater quality assessment of a coastal aquifer using geoelectrical techniques. *J Environ Hydrol* 7:341–349
- Haber E, Oldenburg D (1997) Joint inversion: a structural approach. *Inverse Prob* 13:63–77
- Haeni FP (1986) Application of seismic refraction methods in groundwater modeling studies in New England. *Geophysics* 51:236–249
- Hamdan AH and Vafidis A (2009) Inversion techniques to improve the resistivity images over karstic structures. Proceedings of the 15th European Meeting of Environmental and Engineering Geophysics. 3–5 September 2009, Dublin, Ireland
- Hamdan AH, Kritikakis G, Andronikidis N, Economou N, Manoutsoglou E, Vafidis A (2010) Integrated geophysical methods for imaging saline karst aquifers: a case study of Stylos, Chania, Greece. *J Balkan Geophys Soc* 13:1–8
- Hering A, Misiek R, Gyulai A, Ormos T, Dobroka M, Dersen L (1995) A joint inversion algorithm to process geoelectrical and surface wave seismic data. *Geophys Prospect* 43:135–156
- Imhof AL, Guell AE, Villagra SM (2001) Resistivity sounding method applied to saline horizons determination in Colonia Lloveras-San Juan Province-Argentina. *Brazilian J Geophys* 19(3):263–278
- Jarvis KD, Knight RJ (2002) Aquifer heterogeneity from SH-wave seismic impedance inversion. *Geophysics* 67:1548–1557
- Kuras O, Meldrum PI, Ogilvy RD, Gisbert J, Joretto S, Sanchez MF (2005) Imaging sea water intrusion in coastal aquifers with electrical resistivity tomography: initial results from the lower Andarax delta, SE Spain. In: Proceedings, 11th Annual Meeting EAGE-Near-Surface Geophysics Conference, Palermo, Sicily, Italy
- Lashkaripour GR (2003) An investigation of groundwater condition by geoelectrical resistivity method: a case study in Korin aquifer, southeast Iran. *J Spatial Hydrol* 3(1):1–5 (Fall 2003)
- Lines LR, Schultz AT, Treitel S (1988) Cooperative inversion of geophysical data. *Geophysics* 53:8–20
- Maier D, Maurer HR, Green AG (1995) Joint inversion of related data sets: DC-resistivity and transient electromagnetic soundings. 1st Annual Symposium Environmental and Engineering, Geophysics Society (European Section), (Exp abst.), pp 461–464
- McGillivray P, Oldenburg D (1990) Methods for calculating Fréchet derivatives and sensitivities for the non-linear inverse problem: a comparative study. *Geophys Prospect* 38:499–524
- Mela K (1997) Viability of using seismic data to predict hydrogeological parameters. Presented at SAGEEP, Reno/Sparks, Nevada
- Menke W (1989) Geophysical data analysis: discrete inverse theory. Academic Press, New York
- Michalakis I, Economou N, Hamdan H, Vafidis A, Manoutsoglou E, Panagopoulos G, Roubedakis S, Vozinakis C, Lampathakis S, and Dassysra E (2006) Geological and geophysical study of saltwater contamination at Stylos, Crete. Proceedings of the 2nd International Conference Advances in Mineral Resources Management and Environmental Geotechnology (AMIREG), 25–27 September, Chania, Greece
- Moser TJ (1991) Shortest path calculation of seismic rays. *Geophysics* 56:59–67
- Ogilvy RD, Kuras O, Meldrum PI, Wilkinson PB, Chambers JE, Sen M, Tsourlos P (2009) Monitoring saline intrusion of a coastal aquifer with automated electrical resistivity tomography. In: Proceedings, 15th Annual Meeting EAGE-Near-Surface Geophysics Conference, Dublin, Ireland

- Park SK, Van GP (1991) Inversion of pole–pole data for 3-D resistivity structure beneath arrays of electrodes. *Geophysics* 56:951–960
- Raiche AP, Jupp DLP, Rutter H, Vozof K (1985) The joint use of coincident loop transit electromagnetic and Schlumberger sounding to resolve layered structures. *Geophysics* 50:1618–1627
- Sandberg AK (1993) Examples of resolution improvements in geoelectrical soundings applied to groundwater investigations. *Geophys Prospect* 41:207–227
- Schmutz M, Albouy Y, Guerin R, Maquaire O, Vassal J, Schott JJ, Descloitres M (2000) Joint electrical and time domain electromagnetism (TDEM) data inversion applied to the Super Saube earthflow (France). *Surveys Geophys* 21:371–390
- Singh UK, Das RK, Hodlur GK (2004) Significance of Dar-Zarrouk parameters in the exploration of quality affected coastal aquifer systems. *Environ Geol* 45:697–702
- Soupios MP, Papazaxos CP, Johlin C, Tsokas GN (2001) Nonlinear three-dimensional travelttime inversion of crosshole data with an application in the area of Middle Urals. *Geophysics* 66:627–636
- Soupios P, Kalisperi D, Kanta A, Kouli M, Barsukov P, Vallianatos F (2010) Coastal aquifer assessment based on geological and geophysical survey, northwestern Crete, Greece. *Environ Earth Sci* 61(1):63–77
- Sumanovac F, Weisser M (2001) Evaluation of resistivity and seismic methods for hydrogeological mapping in karst terrains. *J Appl Geophys* 47:13–28
- Tillman A, Stocker T (2000) A new approach for the joint inversion of seismic and geoelectric data. Presented at 63th EAGE Conference and Technical Exhibition, European Association of Geoscience and Engineering, Amsterdam
- Tsourlos P (1995) Modelling, Interpretation and Inversion of Multielectrode Survey Data. PHD Thesis, University of York
- Tsourlos PI, Szymanski JE, Tsokas GN (1998) A smoothness constrained algorithm for the fast 2-D inversion of DC resistivity and induced polarization data. *J Balkan Geophys Soc* 1:3–13
- Vozof K, Jupp DLB (1975) Joint inversion of geophysical data. *Geophys J R Astr Soc* 42:977–991
- Zhang J, Morgan FD (1997) Joint seismic and electrical tomography. Annual Symposium Environmental and Engineering, Geophysics Society (SAGEEP) Exp. Abst., pp 391–395